Renewable Energy 262 (2026) 125373

Contents lists available at ScienceDirect

Renewable Energy

journal homepage: www.elsevier.com/locate/renene

Effect of Nb interlayer thickness on the performance of porous transport layers for proton exchange membrane water electrolyzers

Anurag, Abhay Gupta, Samaneh Shahgaldi *

Hydrogen Research Institute, Université du Québec à Trois-Rivières, Trois-Rivières, G8Z 4M3, Canada

ARTICLE INFO

Keywords:
PEM water electrolyzers
Porous transport layers
Multi-layered coatings
Nb
Interlayers
Polarization curves

ABSTRACT

Polymer electrolyte membrane water electrolyzer (PEMWE) integrated with renewable energy sources is a crucial technology for energy transition. However, the high cost of precious metal-coated porous transport layers (PTLs) is one of the limiting factors for the widespread use of PEMWE. Multi-layered coatings with cost-effective Nb as an interlayer and thin layer of precious metal (one-fourth of commercial) as a top layer could serve as a potential alternative to commercial PTL in PEMWE. This study explored the impact of different thicknesses of Nb interlayer (150, 200, 350 nm) on the electrochemical behavior of multi-layered NbPt coatings, by comparing them with two single layered Pt-coated PTLs (in-house Pt-coated PTL and commercial Pt-coated PTL) under PEMWE simulated condition. The result showed that the Ti PTLs with Nb as an interlayer (150, 200, 350 nm) performed better than the single layered in-house Pt-coated PTL. The best performing multi-layered NbPt (Nb = 350 nm, Pt = 50 nm) sample was finally compared with commercial Pt (200 nm) coated PTL in the in-situ condition of PEMWE. The multi-layered NbPt coating showed an equivalent performance (1.967 V@3.0 A cm^{-2}) compared to commercial Pt coating (1.958 V@3.0 A cm^{-2}), making Nb as a promising cost-effective interlayer for PTL coating.

1. Introduction

Water electrolysis coupled with renewable energy source is the most promising technique available for producing high purity hydrogen (H_2) with zero emission of greenhouse gases during its production route [1]. Proton exchange membrane water electrolyzer (PEMWE) offers the advantage of high current densities, low gasses crossovers, compact design, quick dynamic response and high operating pressure, making them suitable for integration with highly volatile renewable energy source. But due to the higher usage of expensive Pt-group metals (PGMs) in the preparation of stack components, only a small fraction of world H_2 is being produced through PEMWE, limiting its worldwide implementation [2]. Therefore, to reduce the cost of PEMWE, it is crucial to decrease either the operation expenditure (OPEX) or the capital expenditure (CAPEX) by decreasing the overpotential losses and the amount of expensive materials used inside the cell, respectively. The porous transport layer (PTL), a key component of PEMWE, serves as both the electrical and thermal link between the membrane electrode assembly (MEA) and the bipolar plate (BPP). In addition to this, it provides the channels for the movement of water and gas molecules on the anode side of the cell. In view of this, previous studies have investigated the influence of gradient pore structures [3], bubbles dynamics [4,5], clamping pressure [6], etc. on PTL-related OPEX while surface-engineered PTLs [7] have been reported to account for CAPEX.

Due to the presence of harsh oxidizing environment, PTLs are made of corrosion resistant Ti metal, which forms a stable passive layer (TiO_{2-x}) on its surface. But since the interfacial contact resistance (ICR) of the TiO_{2-x} layer deteriorates the performance of PEMWEs, several groups of researchers have previously investigated the use of PGMs-coated PTLs to improve the performance of the cell. For example, Rakousky et al. [8] showed that 78% of the degradation in the cell performance was caused by an increase in ohmic resistance of the uncoated Ti PTL, which on coating with Pt showed lower degradation rate (12 $\mu V\ h^{-1}$) than before (108 $\mu V\ h^{-1}$). Likewise in the separate study [9], it was observed that the surface area of PTL, where the Pt-coating had peeled off, showed an increase in ICR, thereby raising the cell voltage by 50%. Moreover, Liu et al. [10] showed that sputtering Ir on Ti PTL reduced the ICR by 70 $m\Omega\ cm^2$, resulting in an increase in cell performance. Hence based on these studies, it can be stated that to decrease the CAPEX related to PTL coatings, PGMs must be replaced with non-precious transition metals

* Corresponding author.
E-mail address: samaneh.shahgaldi@uqtr.ca (S. Shahgaldi).

https://doi.org/10.1016/j.renene.2026.125373
Received 9 June 2025; Received in revised form 15 January 2026; Accepted 31 January 2026
Available online 2 February 2026

coatings, exhibiting comparable cell performance and durability as former.

The transition metals [11,12] and their respective compounds such as nitrides [13,14], carbides [15], oxides [16,17] etc. have been extensively studied as a coating material for metallic BPPs and PTLs in both proton exchange membrane fuel cells (PEMFCs) and PEMWE. For instance, Lettenmeier et al. [12] investigated the thermally sprayed macro-porous Ti layer on Ti-based PTL in PEMWE. The authors observed an ICR reduction of 20 mΩ cm^2, which in-turn resulted in the higher cell performance for coated Ti PTL (2.6 V@5.0A cm^{-2}) than uncoated Ti PTL (2.75 V@ 5.0A cm^{-2}). Next, Liu et al. [18] nitridated Ti felt to produce TiN/TiO_x composite layer, which leads to an improvement in corrosion resistance (0.920 μA cm^{-2} vs 20 μA cm^{-2}), superior stability (up to 200 h) and lower ICR (1.0 mΩ cm^2 vs 3.20 mΩ cm^2) compared to uncoated Ti felt. However, according to Hwang et al. [19] the PTL performance remains unaffected by variation in Ti powder loading(110, 200 and 300 mg cm^{-3}) on Ti felt. This was attributed to similar flow and bubble size in each case. Next, Fan et al. [16] thermally deposited IrO_2-RuO_2- (0.43 mg cm^{-2})TaO_x on Ti felt with the goal of reducing anode catalyst loading. The authors reported an enhanced performance (1.83 V @ 2.0 A cm^{-2}) at lower loading (1.0 mg cm^{-2}) compared to commercially electroplated Ti felt (1.87 V @ 2.0 A cm^{-2}) operated at higher loading (2.0 mg cm^{-2}). Similarly, in the separate study, Doan et al. [17] demonstrated that spray-coating, followed by thermal treatment of IrO_2 (0.60 mg cm^{-2})/TiO_2 on Ti PTL improved the performance (2.720 A cm^{-2} @2.0 V) compared to uncoated Ti PTL (2.183 A cm^{-2} @2.0 V), indicating prevention of passivation in former. Deng et al. [15] demonstrated that TiC sintered layer on Ti PTL showed better performance compared to uncoated counterpart by 42 mV@2.0 A cm^{-2}, however, no significant difference was observed in their ICR values. Similarly, in the separate study [11], Ti sintered layer on Ti PTL showed an increase in cell performances (2.5 V@2.0 A cm^{-2}) compared to uncoated PTL (2.5 V @6.0 A cm^{-2}), the reported ICR (58 mΩ cm^2@1.4 MPa) was still higher compared to other transition metals such as Nb-based [13] and Ta-based coatings [14]. The reason being the lower conductivity of TiO_2(10^{-6} S cm^{-1}) compared to Nb_2O_5(10^{-4} S cm^{-1}) and $TaO_{x=2.21}$ (1.9×10^{-4} S cm^{-1}), respectively. Moreover, it has been reported [14,20] that besides the conductivity, the corrosion resistance of both sputter-coated Nb-based and Ta-based coatings is also higher than Ti in the PEMWE operating conditions. However, it needs to be mentioned here that these studies lacked crucial simulated lifetime analyses test [16,21], which would have offered a better understanding of the long term durability of the coatings. Nevertheless, the above research findings showcase an excellent protective capabilities of Nb and Ta based coatings in both BPPs and PTLs in PEMWEs; however, their reported ICR values [13,14] were still found to be higher than PGMs coatings [10]. In view of this, multi-layered coatings with Nb or Ta as an interlayer and thin layer of precious metal as the top layer could serve a dual purpose, reducing the CAPEX while also keeping the performance and ICR of coatings in check. Note that in the present study, due to the lower cost of Nb (25% of Ta) compared to Ta, Nb is used as an interlayer between Pt and Ti PTL.

Compared to single layered, multi-layered coatings provide prominent characteristics such as better adhesion, lower residual stress, higher toughness and higher hardness [22,23]. Holleck et al. [23] showed that the cracks generated in the top layer got deflected at the interface of TiC/TiB_2 multi-layered coatings, causing an energy dissipation in interface zone, thereby increasing the toughness of coatings. It has been reported [22] that due to the presence of alternate layers of hard and soft materials, dislocations pile up at the interfaces, resulting in an increase in hardness of the multi-layered coatings. Lastly, because of their compact structure, multi-layered coatings such as TiN/Ti [24] inhibit or delay the diffusion of electrolyte to the substrate, thereby increasing the corrosion resistance of the coatings.

Based on the literature above-mentioned, the objective of the present study is to investigate the role of Nb as an interlayer between Pt (50 nm) and Ti PTL by comparing the electrochemical performances of the each of the samples with and without Nb interlayer. The thickness of Nb interlayer is then investigated to compete with the ex-situ performance of commercial Pt-coated (200 nm) Ti PTL. Finally, the best performing multi-layered NbPt sample is compared with commercial Pt-coated in the in-situ conditions of the PEMWE cell. It is worth mentioning that all the coatings are sputtered through magnetron sputtering technique, which besides being user friendly and cost effective process, is known for producing uniform, dense and well adherent layers. Moreover, to the best of author's knowledge, no prior studies have ever investigated the effects of varying Nb interlayer's thickness on the electrochemical performance of the multi-layered coating. The present study places emphasis on the CAPEX reduction by reducing the loading of PGMs coatings on Ti-based porous transport layers (PTLs). Note that although work [7] has been done in the past to reduce CAPEX related to PTL coatings, the authors [7] focused on lowering Ir loading in catalyst layer by depositing Ir directly on the surface-engineered PTL. Hence the reduced material as well as the procedure adopted for CAPEX reduction significantly differs from that of present study.

2. Materials and methods

In this study, six PTL samples with different configurations are prepared as follows:

First, the water-soluble contaminants were removed from the uncoated PTLs by dipping them in the heated (80 °C) deionized (DI) water for 15 min. Then, they were ultrasonicated in acetone and 2-propanol solution for another 15 min to remove the organic surface contaminations followed by the 15 min reheating in DI water at 80 °C. Finally, they were dried in the air at room temperature [2].

Next, DC magnetron sputtering was used to deposit Nb and Pt on the uncoated PTLs. The deposition power, base pressure and working pressure were kept at 150 W, 1.33×10^{-4} Pa and 6.66×10^{-1} Pa, respectively. Since the sputtering procedure adopted was thickness-controlled, a 14 mm gold crystal was used to monitor the thickness of the sputtered material. Table 1 shows the detailed information about the materials and coatings used in each of the 6 cases of PTLs whereas Fig. 1 displays their schematic forms.

Thermo Scientific Helios 5, a focussed ion beam instrument was then used to measure the thickness of the coated materials through cross sectional imaging. Fig. S1 in the Supplementary Information shows the milling operation.

It is to be noted that the corrosion (open circuit potential (OCP), potentiodynamic and potentiostatic/chronoamperometry (CA) polarization, simulated lifetime test) and characterization (scanning electron microscopy (SEM), energy dispersive x-ray spectroscopy (EDS), x-ray photoelectron spectroscopy (XPS), surface roughness and ICR before and after corrosion tests) techniques used in this study are discussed in detail at the end of the Supplementary Information.

Table 1
Types of samples investigated in the current work.

Sample name	Sample details
UN-Ti	Uncoated Ti PTL (2GDL06N-015 BQ), purchased from Bekaert
SL-Pt	Single layered coating of Pt (50 nm) on Ti PTL
ML-1	Multi-layered coating, with Nb as an interlayer (150 nm) and Pt as a top layer (50 nm) on Ti PTL.
ML-2	Multi-layered coating, with Nb as an interlayer (200 nm) and Pt as a top layer (50 nm) on Ti PTL.
ML-3	Multi-layered coating, with Nb as an interlayer (350 nm) and Pt as a top layer (50 nm) on Ti PTL.
CM-Pt	Commercially coated PTL (Bekaert 2GDL06N-0150-PT200), with single layer of Pt (200 nm)

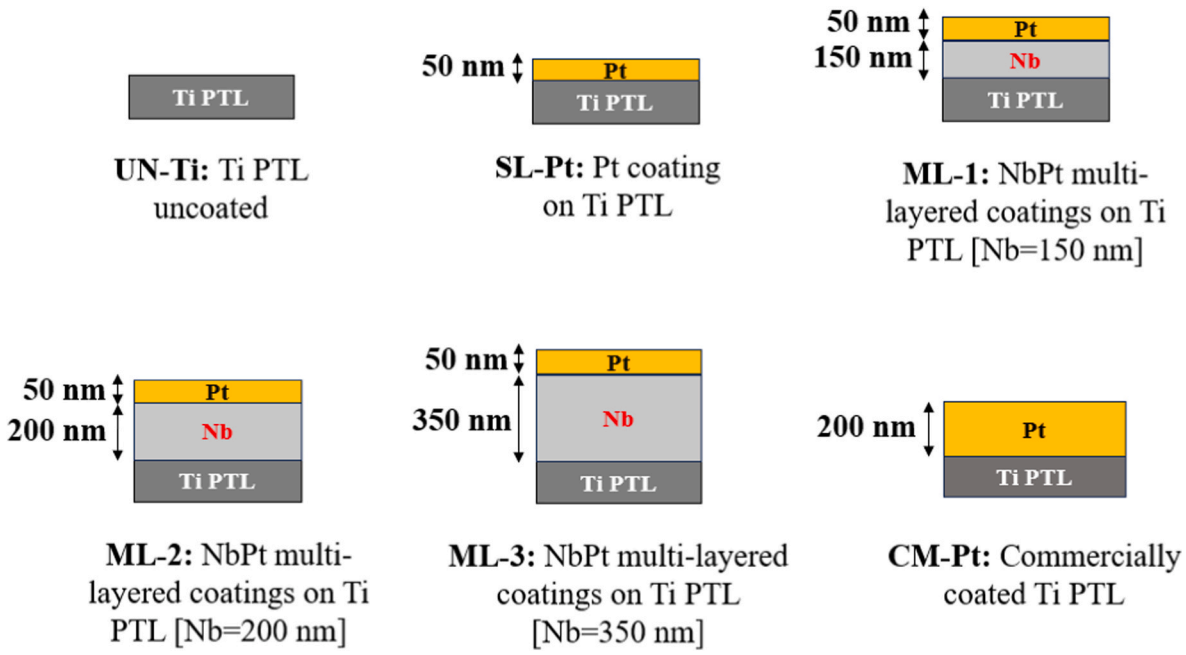

Fig. 1. Schematic of each of the six samples with their respective coatings' thicknesses.

3. Results and discussion

3.1. Surface characteristics

Fig. 2 shows the SEM micrographs of surface of all the samples. Fig. 2a represent the surface morphology of the uncoated Ti PTL (UN-Ti). Fig. 2b–e shows that in the case of sputtered coated samples, the top surfaces of Pt have no visible cracks, pores or pinholes. The coatings look compact and are uniformly distributed across the surface. Moreover, since all the sputtered samples are well-bonded and have sharp interfaces between them (Fig. 3), Ti, Nb, and Pt seems to be well-adhered with each other in all the samples. Based on all the above observations, it can be assumed that these coatings will prevent the surface passivation of Ti by acting as a barrier between the Ti substrate and the acidic medium, present inside the PEMWE cell. The SEM micrographs of each of the samples at 100× magnification are shown in the Supplementary Information (Fig. S2). It should be noted that since commercial CM-Pt is deposited using an electroplating method, its morphology (Fig. 2f) seems completely different from sputter-coated samples. However, because of the limited information regarding the coating parameters used in the case of CM-Pt, the authors refrain from making any comments on its surface morphology.

3.2. Electrochemical tests

3.2.1. Open circuit potential (OCP) measurement

OCP is used to measure the corrosion potential, which gives an idea about the thermodynamic susceptibility of material towards corrosion. Fig. 4 shows the OCP curves for the uncoated/coated samples. The order of OCP values after 4.0 h of exposure is UN-Ti (−1.15 V) < SL-Pt (0.125

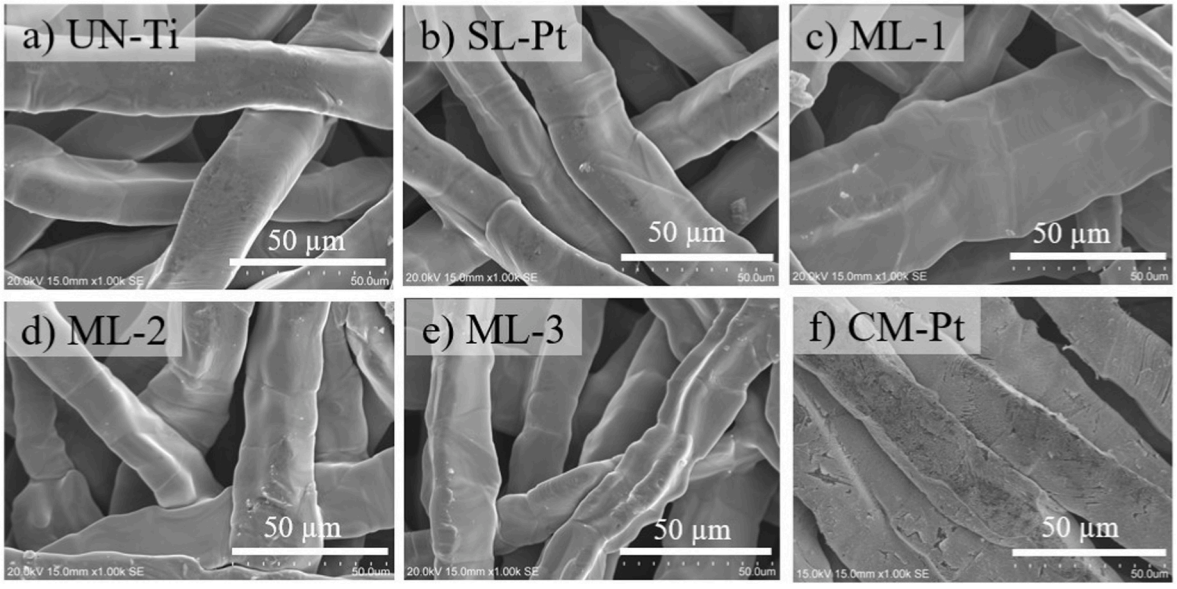

Fig. 2. Scanning electron microscopy (SEM) images of surface of each of the pristine samples at 1000× magnification.

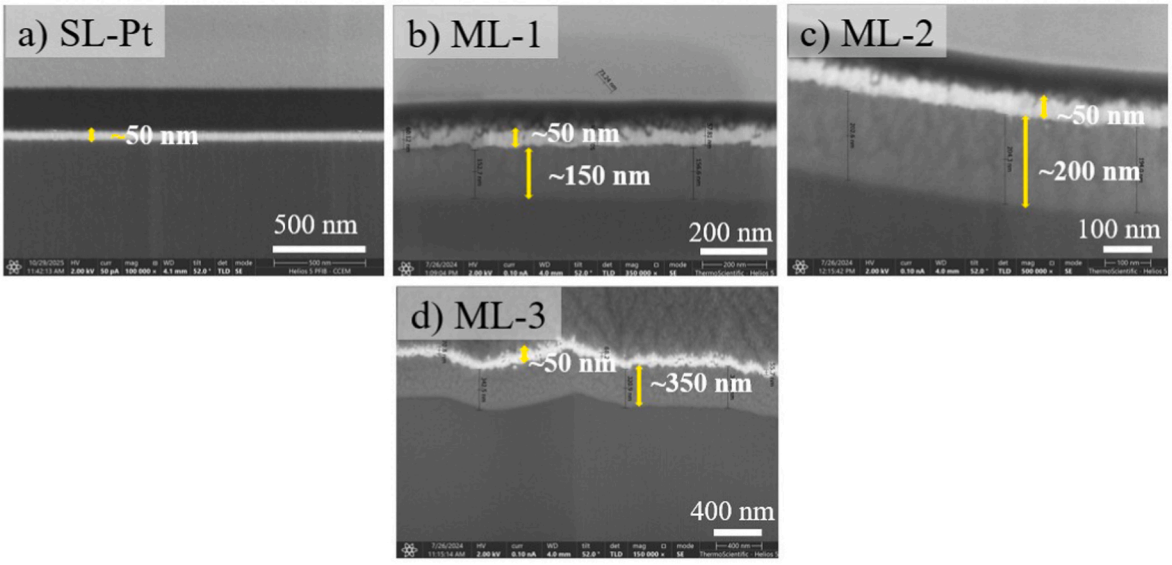

Fig. 3. Coating thickness for SL-Pt, ML-1, ML-2 and ML-3 samples, measured through FIB-SEM cross-section imaging technique.

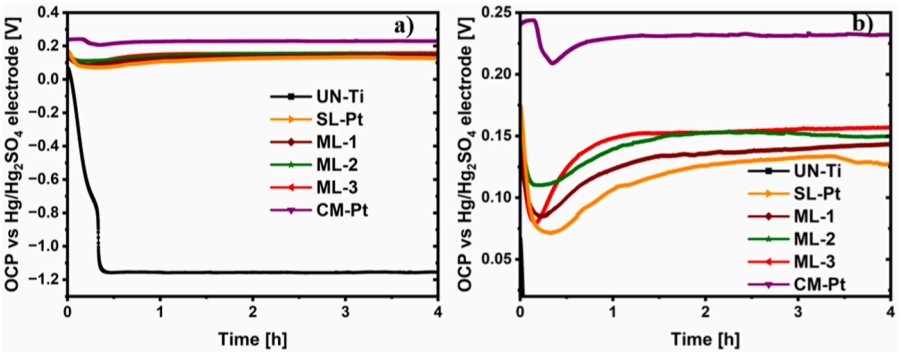

Fig. 4. (a) Open circuit potential (OCP) curves of the samples in 0.5 M H_2SO_4 solution at 80 °C (b) Enlarged view for SL-Pt, ML-1, ML-2, ML-3 and CM-Pt depicting the OCP and stability time for each sample.

V) < ML-1 (0.142 V) < ML-2 (0.148 V) < ML-3 (0.157 V) < CM-Pt (0.232 V). It implies that thermodynamically, the samples with Nb as an interlayer (ML-1, ML-2 and ML-3) are less susceptible to corrosion than the sample with no Nb i.e. SL-Pt. Moreover, as the Nb thickness increases, anti-corrosion tendency of the sample increases. Besides this, the OCP value of CM-Pt and ML-3 stabilizes earlier (1.0 h) than the ML-2 (2.0 h) and ML-1 (3.2 h), which indicates the faster kinetics of oxide formation on the surface of the former. Interestingly, SL-Pt hasn't reached the complete stability even after 4.0 h of exposure, which can be explained by the study done by Chipatecua et al. [25] They reported that in the case of magnetron sputtered Cr/CrN on steel substrate, the sample with lower coating thickness allows the electrolyte to reach the substrate earlier than the higher thickness multi-layered coated samples. In view of this, similar phenomenon could be assumed to be true for SL-Pt. Due to the lowest thickness of SL-Pt, the continuous formation of TiO_{2-x} passive film delays the position of voltage stability in the OCP curve. It is to be noted that the above-mentioned explanation is only valid for sputtered coated samples as electroplated CM-Pt sample, despite having lower total thickness (200 nm), stabilizes earlier than ML-2 (250 nm) sample. The reason behind this is unclear but could be attributed to lower pinhole density in CM-Pt compared to ML-2. As sputtering is a 'line of sight' depositing process, the possibility of shadowing increases during the sputtering process. Since the surface of the Ti PTL is intrinsically rough (as observed in Fig. 2a), the shadowing effect results in a non-uniform coating of the substrate area, prompting the generation of micro-pinholes. These pinholes then allow the electrolyte to reach the substrate, resulting in galvanic corrosion of lesser noble metal among the coating and substrate. However, in the case of electroplating technique, samples are usually submerged in an electrolyte solution containing the metal ions that needs to be deposited. Hence, the probability of metal ions penetrating the shadowed region of PTL fibers increases, resulting in a uniform coating all across the PTL. In view of this, faster stability of OCP in the case of electroplated CM-Pt could be attributed to its lower pinhole's density compared to ML-2. Moreover, before depositing any metal through electroplating, researchers typically employ acid 'pickling' treatment to remove Ti oxide passive layer by immersing them in appropriate etching solution. Besides oxide removal, Singh et al. [26] has shown that the electrochemical etching of Ti PTL (before electroplating Au) results in titanium hydride (TiHx) formation on Ti surface. Since the formed TiH_x prevents the excessive re-oxidation of Ti, electroplated CM-Pt sample (assuming pickling as a pretreatment) will provide better kinetic stability compared to sputter-coated ML-2 sample. Note that this statement is only valid if the electrolyte has reached the substrate in both CM-Pt and ML-2, as ML-3 (despite being sputter-coated) shows rapid OCP stability (1.0 h) with no fluctuation in voltage, indicating no evidence of electrolyte penetration. Nevertheless, because of the limited information about the pretreatment and pinhole density of CM-Pt compared to sputter-coated ML-2, the exact cause remains uncertain.

It is to be noted that despite the above advantages, electroplating is

not feasible for Nb metal deposition in aqueous solution. This is due to the preferential evolution of H_2 (0 V) compared to Nb reduction reaction (Nb^{+5}/Nb (−0.96 V vs SHE); Nb^{+3}/Nb(−1.10 V vs SHE)), which leads to hydrogen embrittlement [27]. Moreover, due to its high affinity for oxygen, Nb is prone to oxidation during electroplating [28,29]. To tackle this issue, researchers have tried to electroplate Nb in non-aqueous solution. However, these methods require high temperature (>750 °C) and complex multistep pretreatments involving cyanide bath [28], causing environmental contamination [29]. Hence, Nb sputtering (in the current study), not only mitigates oxidation (Nb and Pt are coated sequentially without breaking vacuum) but also offers a user friendly and cost effective alternative.

3.2.2. Potentiodynamic polarization measurement

Potentiodynamic polarization curve for the UN-Ti, SL-Pt, ML-1, ML-2, ML-3 and CM-Pt samples is shown in Fig. 5. During the potentiodynamic polarization test, the potential of the working electrode is varied while the corresponding current density is being recorded to evaluate the kinetic parameters of the corrosion process (Table 2). Tafel slopes (β_a and β_c) are determined using EC lab software, within 60 mV range on either side of the E_{corr} while the I_{corr} and R_P are obtained using Tafel extrapolation method and Stern-Geary equation respectively. Since, Ti has a higher affinity for O_2 than that of Pt, the uncoated PTL (UN-Ti) has the lowest R_P than all the coated samples (Table 2). Note that, at this point of a time, no comparison can be made between the corrosion resistance of ML-1, ML-2 and ML-3 since the R_P values in each of the cases are quite similar. However, it is evident from Table 2, that all the samples with Nb as an interlayer (ML-1, ML-2 and ML-3) showed greater R_P values than the sample without Nb interlayer (SL-Pt and CM-Pt). The possible reasons behind this are explained hereafter, separately for SL-Pt and CM-Pt samples. First, due to the shadowing effect in the case of sputtered SL-Pt (as discussed in section 3.2.1), the generated pinholes will allow the electrolyte to reach the substrate, resulting in galvanic corrosion of Ti. Hence it can be stated that the corrosion of Ti gets accelerated because of the large cathodic area provided by the noble metal Pt, present on the surface. In view of this, use of Nb as an interlayer eventually breaks the continuity of pores and pinholes, which leads to the formation of densely compacted structure in multi-layered coatings compared to single layered counterpart. The second possible reason could be attributed to the poor adhesion of Ti with Pt (in SL-Pt and CM-Pt sample) compared to the adhesion of Nb with Pt and Ti in the multi-layered samples, which would again contribute to galvanic coupling in the case of former. It is to be noted that the issue related to the adhesion of Pt and Ti will be discussed in depth in section 3.4.

3.2.3. Potentiostatic polarization (CA) measurement

To investigate the corrosion resistance of PTLs in the anodic PEMWE operating condition, the potentiostatic polarization test was conducted in 0.5 M H_2SO_4 solutions for 6.0 h under application of constant voltage of 2.0 V [2,30]. Fig. 6a shows the CA curves for the uncoated/coated samples. The order of current densities after 6.0 h of CA is CM-Pt (137 mA cm^{-2}) > SL-Pt (126 mA cm^{-2}) > ML-1 (100 mA cm^{-2}) > ML-2 (94 mA cm^{-2}) > ML-3 (90 mA cm^{-2}) > UN-Ti (0.68 mA cm^{-2}). It is to be noted that although the current density of CM-Pt is higher than all the sputtered coated samples, it doesn't specify the lower corrosion resistance in the case of former. According to the study done by Gupta et al., [30] the current density in CA, is a combination of both metal oxidation and the oxygen evolution reaction (OER), which in turn depends on the surface roughness and percentage of Pt-coated area. In view of this, higher OER activity in the case of CM-Pt could be attributed to the large percentage of Pt-coated area compared to sputter-coated samples. As seen from Fig. S3a and b, the fibers located in the deeper section of commercial PTL are also coated with Pt, however in the case of Fig. S3c and d, sputtering is confined to the top surface. These observations are consistent with the typical methodology adopted for electroplating deposition (as discussed in section 3.2.1). Since samples are submerged in an electrolyte solution, the metal ions penetrate through the PTL pores, resulting in a uniform coating all across the PTL. Similar phenomenon is likely to hold in the case of CM-Pt, which explains its higher OER compared to sputtered coated sample. However, based on the roughness data (Fig. S4) of CM-Pt (Average roughness (Sa) = 7.99 μm) and SL-Pt (Sa = 9.21 μm), OER should have been higher for sputtered coated SL-Pt. The contrary results indicates higher contribution of Pt-coated fibers (present below the surface) to the overall OER in the case of CM-Pt. Nevertheless, CA was performed at 1.0 V for coated samples to remove the contribution of OER (since minimum required voltage for OER is 1.23 V). Fig. 6b shows that the order of current densities after 6.0 h of CA at 1.0 V is SL-Pt (0.029 mA cm^{-2}) > CM-Pt (0.024 mA cm^{-2}) > ML-1 (0.013 mA cm^{-2}) > ML-2 (0.012 mA cm^{-2}) ~ ML-3 (0.012 mA cm^{-2}). However, since Pt-coated area (including inner fibers) is greater in CM-Pt (as discussed above), the exposed surface would be significantly greater than 1.0 cm^2. As a result, the current density (shown above) is an overestimated value (since it's been divided by 1.0 cm^2), which still does not indicate the true corrosion behavior of CM-Pt. Hence for comparison of samples with different Pt-coated area or electrochemical surface area, the evaluation of SEM images after CA would provide a better picture of corrosion resistance rather than analyzing CA data. It can be observed from Fig. 7 and Fig. S5 (at lower magnification) in the supplementary information, CM-Pt shows higher amount of peeling than multi-layered samples i.e. ML-1, ML-2 and ML-3, indicating lower corrosion resistance in commercial PTL.

Contrary to the CM-Pt, all the sputtered coated samples (SL-Pt, ML-1, ML-2 and ML-3) could be assumed to have identical top layer (Pt) with similar roughness, which suggests that the activity of OER must be uniform in all the sample. Therefore, the difference in the current density, as seen in Fig. 6a would solely be due to the resistance provided by the coating. This explains the similar order of current density for sputtered coated samples in both Fig. 6a and b. It can be concluded that the corrosion resistance of each of the samples with Nb as an interlayer (ML-1, ML-2 and ML-3) is greater than the sample without Nb i.e. SL-Pt.

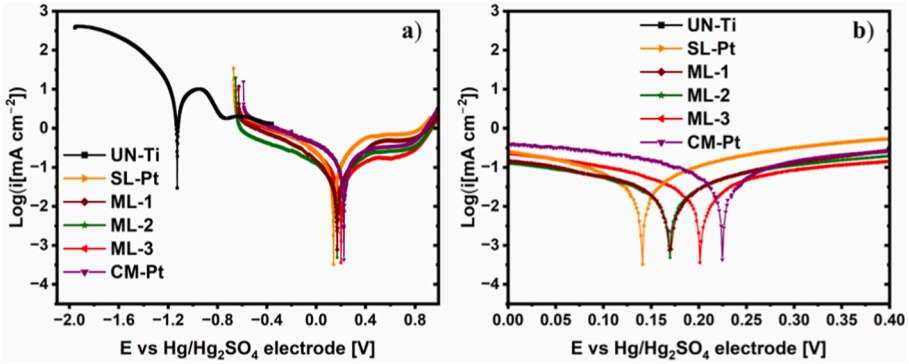

Fig. 5. (a) Potentiodynamic polarization curves of the samples in 0.5 M H_2SO_4 solution at 80 °C (b) Enlarged view for SL-Pt, ML-1, ML-2, ML-3 and CM-Pt.

Table 2
Electrochemical parameters (mean ± standard deviation) of all the samples obtained from Tafel plot (potentiodynamic polarization curve).

Samples	E_{corr} [V]	I_{corr} [μA cm^{-2}]	β_a [mV decade^{-1}]	β_c [mV decade^{-1}]	R_p [Ω cm^2]
UN-Ti	−1.125 ± 0.077	2404.08 ± 138.35	157 ± 5	89 ± 2	10.3 ± 0.7
SL-Pt	0.141 ± 0.012	19.85 ± 1.15	105 ± 2	100 ± 3	1119.1 ± 70.8
ML-1	0.170 ± 0.007	16.96 ± 0.58	103 ± 4	125 ± 2	1445.6 ± 51.5
ML-2	0.172 ± 0.004	16.96 ± 0.65	109 ± 3	125 ± 5	1492.4 ± 59.6
ML-3	0.204 ± 0.018	13.12 ± 0.39	92 ± 2	91 ± 1	1518.2 ± 44.3
CM-Pt	0.224 ± 0.011	22.24 ± 0.71	133 ± 6	131 ± 4	1287.9 ± 68.1

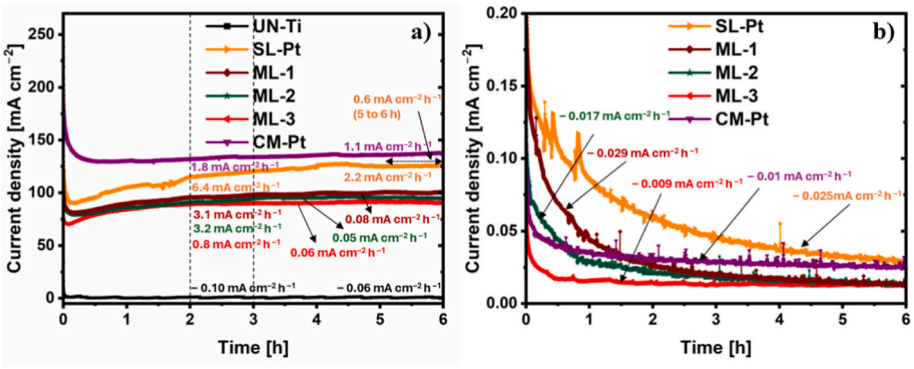

Fig. 6. Potentiostatic polarization curves along with their degradation rate for (a) all samples at 2.0 V and (b) coated samples at 1.0 V in 0.5 M H_2SO_4 solution at 80 °C.

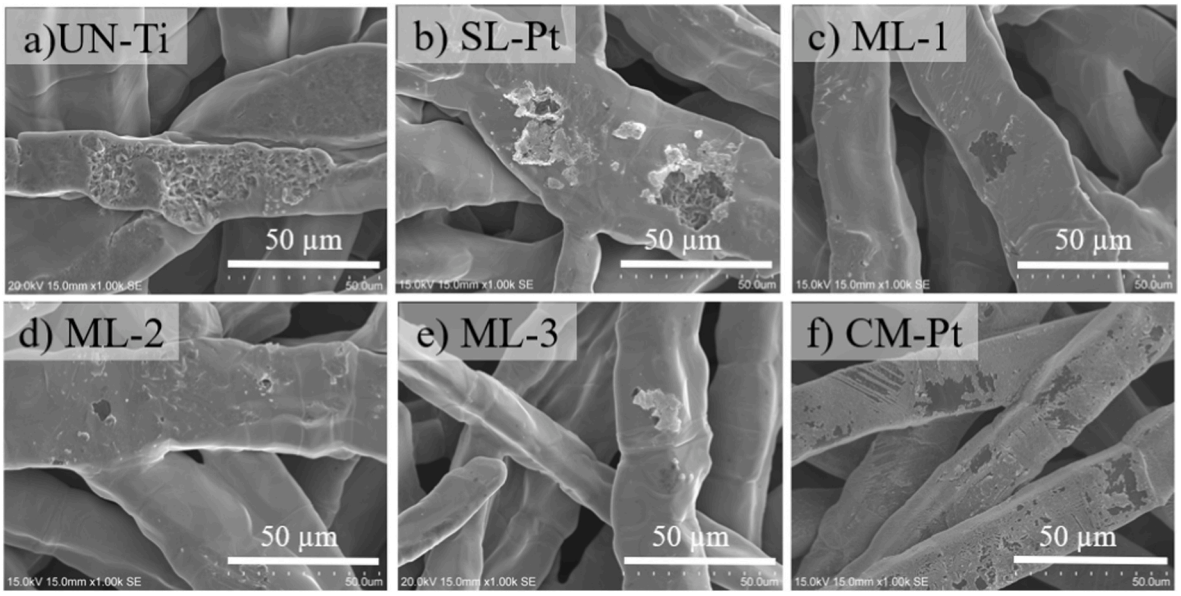

Fig. 7. (a–f) represents the Scanning electron microscopy (SEM) images of UN-Ti, SL-Pt, ML-1, ML-2, ML-3 and CM-Pt, respectively after the chronoamperometry (CA) test of 6.0 h.

Moreover, based on the degradation rates of less than 0.001 A cm^{-2} h^{-1} (Fig. 6a), the current density values in case of ML-3 (2.0 h), ML-2 (3.0 h) and ML-1 (3.0 h) stabilize much earlier than SL-Pt (5.0 h), further confirming the galvanic corrosion protection in the multi-layered cases. These trends are consistent with the SEM micrographs (Fig. 7) obtained after CA for each of the cases. It is observed that in the case of SL-Pt (Fig. 7b), top layer of Pt is chipped off from the certain places compared to the much lesser peeling in the case of ML-1, ML-2 and ML-3 (Fig. 7c–e), indicating lower corrosion resistance of former than the latter.

However, it should be noted that in the case of SL-Pt and CM-Pt, even though the peeling is greater than that of samples ML-1, ML-2 and ML-3, most of the coating remains intact even after 6.0 h of CA (Fig. S5b and f in the Supplementary Information). We therefore increased the time of CA to 15 h to examine the degradation behavior of each sample in a more effective way. But even after 15 h of CA, no appreciable difference was found in the overall coating morphology of any of the samples (Fig. S6 in the Supplementary Information) except for a few places in the case of SL-Pt and CM-Pt where significant peeling was observed. These higher durability of the samples at 2.0 V can be explained based on results of simulated lifetime (SLT) analysis (will be discussed in section 3.4) of each of the samples. It is observed that during the SLT test, each sample lasted for more than 34 h at the externally applied current density of 2.0 A cm^{-2}, which results in a much higher voltage output

than the constant 2.0 V_{RHE} that was employed in the CA test. Therefore, it is evident that even if the duration of CA is increased by few hours, it is highly likely that the coating will remain intact, and the observable corrosion would be negligible. Hence, it can be stated that the SEM results (obtained after CA test) are not conclusive enough to compare the corrosion resistance of ML-1, ML-2 and ML-3 with each other. Moreover, the final current densities i.e. 100, 94 and 90 mA. cm^{-2} @ 2.0 V and 0.013, 0.012 and 0.012 mA. cm^{-2} @ 1.0 V respectively for each of these three samples are relatively similar after 6.0 h. Hence, SLT test is needed to observe the appreciable change in the surface characteristics of the samples.

3.3. Interfacial contact resistance (ICR) measurement

Besides having superior corrosion resistance, PTL must have low ICR to reduce the ohmic overpotential inside the PEMWE. It has been reported that the ICR at MEA/PTL and BPP/PTL interfaces is the main cause of ohmic overpotential, which directly affects the cell performance [30]. Fig. 8 indicates the ICR of all the six samples both before and after 6.0 h of polarization (CA) test. The light blue region highlights the range of clamping pressures (1.2–2.0 MPa) that are most frequently used inside the commercial PEMWE stack. In Fig. 8a, the order of the ICR for the entire range of clamping pressure is UN-Ti > ML-3 > ML-2 > ML-1 > SL-Pt > CM-Pt. Since the electrical conductivity of TiO_2 (10^{-6} S cm^{-1}) passive layer is lower compared to the Pt metal (10^5 S cm^{-1}), the ICR is observed to be higher in the case of UN-Ti than the coated samples. In addition to this, it can be observed that as the thickness of Nb increases, the ICR of the coating increases in the case of multi-layered samples. It is to be noted that in the case of single layered samples, despite having higher thickness of Pt (200 nm), the CM-Pt is observed to have lower ICR than that of SL-Pt. The reason behind this is unclear but could be attributed to lower roughness of CM-Pt compared to SL-Pt (Fig. S4), which would lead to higher contact area and reduced ICR in former. Nevertheless, similar decrease in ICR with increase in Ir loading was reported by Liu et al. [31] in their study on Ti PTLs. The authors associated this behavior with lower loading on Ti PTLs. Apart from this, based on the assumption that CM-Pt underwent acid 'pickling' treatment before electroplating, the higher electrical conductivity of TiH_x (1.16×10^6 Ω^{-1} m^{-1}) compared to TiO_2 (10^{-4} Ω^{-1} m^{-1}), could be attributed to lower ICR of CM-Pt compared to SL-Pt (here Pt was coated on bare Ti felt without etching). Please note that the amount of TiH_x on the surface of Ti would also depend on the duration of pickling. Hence the insufficient treatment of CM-Pt may contain residual Ti phase, which can still be oxidized to TiO_2 through air or electrolyte penetration.

Next, Fig. 8b shows the ICR of all the samples after 6.0 h of polarization (CA) test. The order of ICR remains same except SL-Pt exhibited higher ICR compared to ML-1 and CM-Pt sample in the range of 1.2–2.0 MPa. The reason behind this could be linked to the lower amount of galvanic corrosion in ML-1 and CM-Pt compared to SL-Pt, which due to its lower thickness allows the electrolyte to reach the substrate earlier than that of the former. Nevertheless, the ICR of all the coatings meet the U.S. Department of Energy technical target for fuel cell (similar value of technical target might be anticipated for electrolyzers as well), reconfirming the fact that there is a negligible corrosion after 6.0 h of CA at 2.0 V. The ICR at 1.4 MPa for UN-Ti, SL-Pt, ML-1, ML-2 and ML-3 and CM-Pt before CA (Fig. 7a) is 5.34 mΩ cm^2, 0.73 mΩ cm^2, 1.54 mΩ cm^2, 1.74 mΩ cm^2, 1.88 mΩ cm^2 and 0.52 mΩ cm^2, respectively, which after CA (Fig. 7b) has risen to 8.12 mΩ cm^2, 2.47 mΩ cm^2, 2.15 mΩ cm^2, 2.47 mΩ cm^2, 2.67 mΩ cm^2 and 1.79 mΩ cm^2, respectively.

3.4. Simulated lifetime test

Simulated lifetime test (Fig. 9) is performed at 2.0 A cm^{-2} to compare the long-term durability of each of the samples. It is observed that the order of durability obtained using the SLT is ML-3 (102 h) > CM-Pt (68 h) > ML-2 (59 h) > ML-1 (45 h) > SL-Pt (35 h) > UN-Ti (2.5 min).

UN-Ti shows life span of only ~2.5 min (Fig. 9b), indicating the early formation of non-conductive TiO_{2-x} oxide layer, which caused a rapid surge in the output voltage. Next, the lower SLT (35 h) for SL-Pt compared to other multi-layered samples can be explained by the higher amount of galvanic corrosion between Ti and Pt in the former than the latter. This statement is consistent with the SEM (Back scattered electron (BSE)) micrographs of SL-Pt (Fig. 10a) and ML-1 (Fig. 10c) after 35 h of exposure time, which is also the SLT for SL-Pt. At first glance, it looks like that even after 35 h, there is no peeling or spalling of the Pt coating in the case of SL-Pt whereas the ML-1 shows considerable amount of peeling off the surface. However, EDS image (Fig. 10b) shows that in the case of SL-Pt, the considerable amount of Pt is being removed and only traces of Pt are left, compared to the higher amount of Pt observed in ML-1 (Fig. 10d). Therefore, the smooth surface observed in the case of SL-Pt is not Pt but the TiO_{2-x} passive layer. This indicates that the Pt has relatively better adhesion with Nb compared to that with Ti, which explains the higher amount of galvanic corrosion, as mentioned above, in SL-Pt compared to other multi-layered samples. The complete EDS mappings and quantitative analysis of all the elements present in SL-Pt and ML-1 are provided in Figure S7 and Figure S8, respectively of the Supplementary information. Note that the higher adhesion of Nb with Ti can be explained by its ability to strongly react with TiO_2 even at room temperature. It has been reported [32] that during the early stage of growth, Nb forms 0.6 nm of NbO_x layer by reducing 2–3 nm of TiO_2 to Ti_2O_3 at Nb/TiO_2 interface. The Gibbs free energy (ΔG) for the formation of NbO, NbO_2 and Nb_2O_5 are −36 kJ mol^{-1}, −57 kJ mol^{-1} and −59 kJ mol^{-1}, respectively at 25 °C. Furthermore, the transition layer between NbO_x and reduced TiO_2 was found to be 1 nm, indicating interdiffusion between two species. A similar reaction at the Nb/Al_2O_3 [33] interface at 600 °C, has been shown to enhance the adhesion of Ag to the

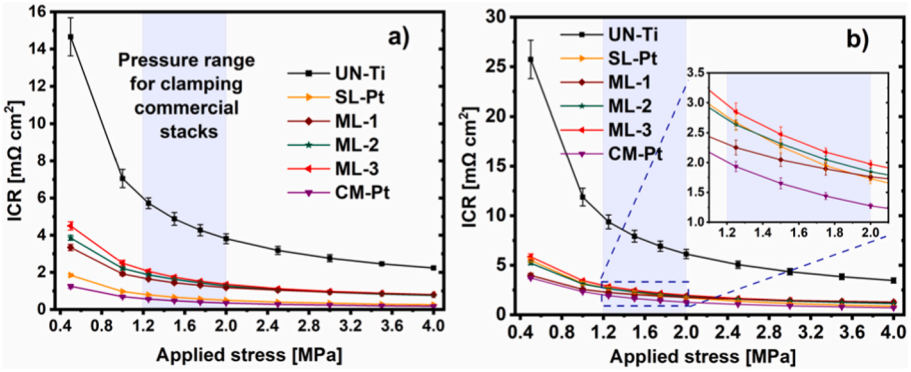

Fig. 8. Interfacial Contact Resistance (ICR) measurements of UN-Ti, SL-Pt, ML-1, ML-2, ML-3 and CM-Pt (a) before and (b) after 6.0 h of chronoamperometry (CA). The error bars represent the standard deviation associated with each value.

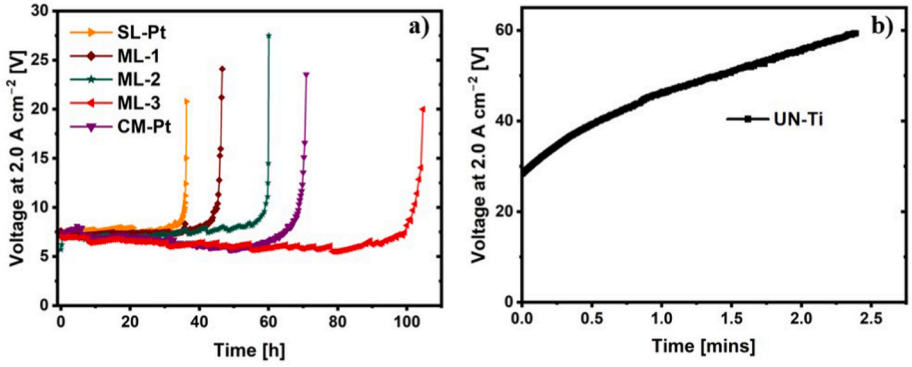

Fig. 9. Simulated Lifetime of (a) SL-Pt, ML-1, ML-2, ML-3, CM-Pt and (b) UN-Ti @ 2.0 A cm^{-2} in 0.5 M H_2SO_4 solution at 80 °C.

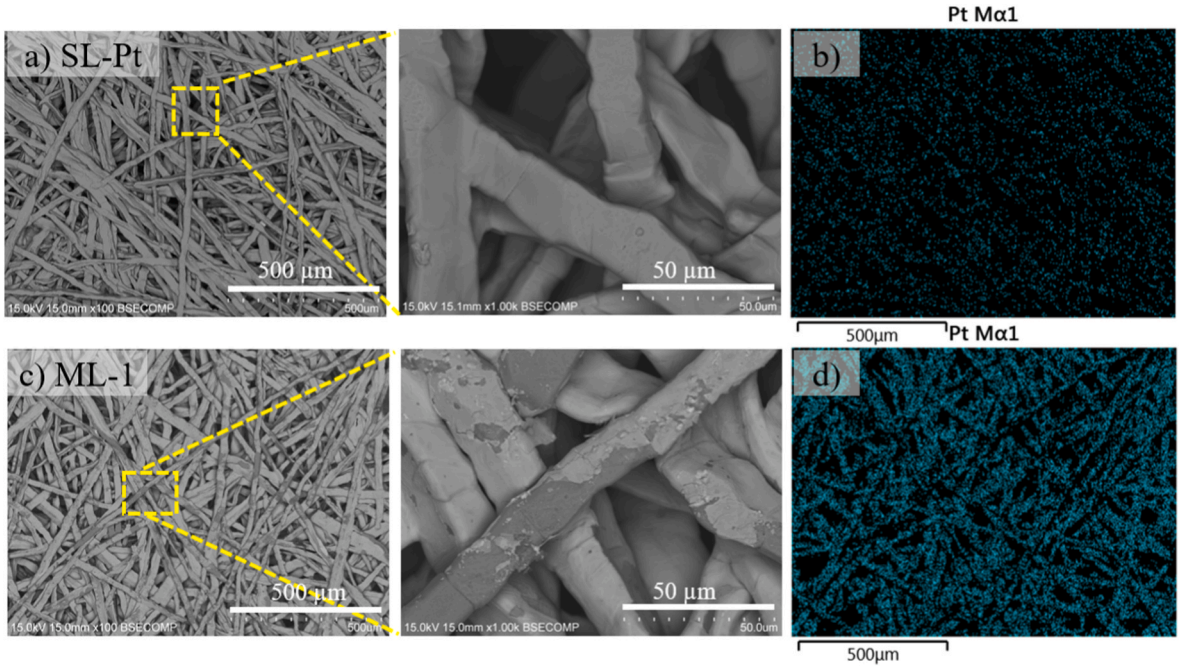

Fig. 10. Comparison of morphology of SL-Pt and ML-1 after 35 h of exposure time @ 2.0 A cm^{-2} using (a, c) SEM (Back scattered electron (BSE) image) and (b, d) Energy dispersive x-ray spectroscopy (EDS) mapping (Pt).

Al_2O_3 substrate on the application of Nb interlayer. In view of this, while thin passive layer of TiO_2 on Ti PTL typically reduces the adhesion with other metals, it enhances the adhesion with Nb. The statement is consistent with the high SLT of multi-layered samples, particularly ML-3. Note that although the mechanism behind an enhanced adhesion in Nb and Pt is unknown, Chellehbari et al. [34] has confirmed the excellent adhesion of sputtered Pt on Nb-based bipolar plates.

Despite being a single layered Pt coating, CM-Pt performs better than two of the multi-layered samples i.e. ML-1 and ML-2, which seems counterintuitive from the perspective of galvanic corrosion. Therefore, to understand the reason behind this, the SEM (BSE) micrographs (Fig. 11a–c) of ML-2 and CM-Pt are compared after their respective SLT i.e. after 59 h and 68 h, respectively. It is observed that in the case of CM-Pt, like SL-Pt, top layer of Pt is peeled off to a greater extent compared to ML-2, where negligible peeling is observed on the surface. However, the total amount of retained Pt (including the inner fibers) in CM-Pt may still be comparable to the Pt in ML-2, where coating is restricted to top surface (Fig. S9). Hence XPS is done (Fig. 11b–d) to investigate the oxidation state of Pt on each of their surfaces after the SLT tests. The characteristic peak positions for the Pt 4f 7/2 electron peaks of Pt (0), Pt $(OH)_2$ (+2), PtO (+2) and PtO_2 (+4) are 71.4 eV, 72.6 eV, 72.3 eV, and 74.6 eV, respectively with each having spin orbit splitting (Δ) of 3.3 eV. Table 3 shows that in the case of ML-2, all the Pt is oxidized to PtO (41.99 %) and PtO_2 (58.01 %) whereas in the case of CM-Pt, 40.87% of the Pt is still unoxidized and the rest is oxidized to $Pt(OH)_2$ (35.96%), and PtO_2 (22.17%), respectively. Since the conductivities of Pt(+2) (10^3 S cm^{-1}) and Pt(+4) (1.0 S cm^{-1}) are lower compared to Pt(0) (10^5 S cm^{-1}) [35], CM-Pt coating (assuming a similar area coverage as ML-2) facilitates enhanced electron transport by providing additional conductive pathways compared to ML-2. This explains the earlier point of voltage surge in case of ML-2 than CM-Pt. Nevertheless, ML-3 shows the higher SLT (102 h) compared to CM-Pt (68 h), which is supported by the SEM (BSE) images (Fig. 11c–e) of both the samples after 68 h of exposure time. It is observed that in the case of ML-3, in addition to the negligible peeling, most of the Pt (94.96 %) (Table 3) is still unoxidized, thereby resulting in the higher SLT compared to CM-Pt. However, to understand the corrosion mechanism in multi-layered and single layered coatings, cross-sectional analysis (Fig. 12) is done for ML-2, CM-Pt and ML-3 after 59 h, 68 h, 68 h, respectively. ML-2 (Fig. 12a) exhibits nanoscale voids (highlighted in red circle), indicating electrolyte penetration into Ti substrate. The observation aligns with the presence of TiO_2 peaks at Nb/Ti interface after 59 h (Fig. S10a). Moreover, the

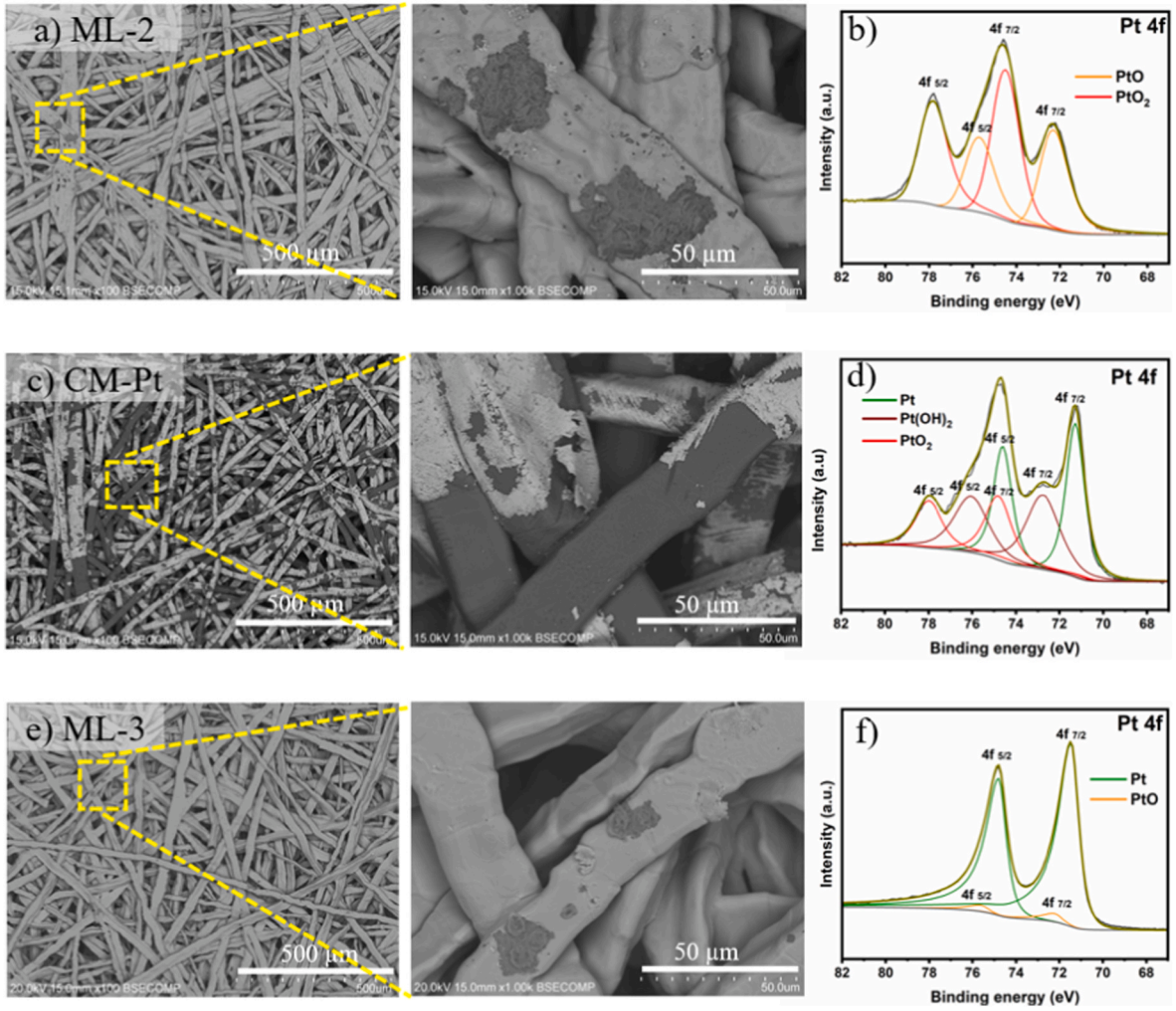

Fig. 11. Comparison of morphology of ML-2, CM-Pt and ML-3 after 59 h, 68 h and 68 h of exposure time, respectively @ 2.0 A cm^{-2} using (a, c, e) SEM (BSE image) and (b, d, f) X-ray photoelectron spectroscopy (XPS) technique.

Table 3
X-ray photoelectron spectroscopy (XPS) quantitative analysis data (atomic %) of Pt and its oxides for ML-2, CM-Pt and ML-3 after 59 h, 68 h and 68 h of SLT, respectively.

Samples	Pt [%]	PtO [%]	$Pt(OH)_2$[%]	PtO_2 [%]
ML-2	–	41.99	–	58.01
CM-Pt	40.87	–	35.96	22.17
ML-3	94.96	5.04	–	–

thickness of top layer is found to be greater than 50 nm(Fig. 12b), which could be attributed to expansion caused by Pt oxides in ML-2 (Fig. 11b). Note that due to the non-uniformity and intermixing of Pt and Nb at Pt/Nb interface, the actual thickness may vary slightly than being reported here. Next, compared to ML-2, CM-Pt (Fig. 12c) shows accelerated Ti degradation, indicating higher amount of galvanic corrosion (discussed in section 3.2.2) in latter. A similar mechanism of micro-galvanic corrosion has been reported by Feng et al. [36] in the case of epoxy coatings. Nevertheless, the difference in corrosion of CM-Pt and ML-2 can be explained by the greater potential difference (ΔE_{corr}) between Pt/Ti metals (0.224 V vs −1.125 V) (Table 2) than that between Pt/Nb (0.224 V vs −0.452 V) and Nb/Ti (−0.452 V vs −1.125 V) [34] metals in 0.5 M H_2SO_4 solution at 80 °C. In addition, the thickness of Pt (Fig. 12d) is found to be lower than 200 nm, which is a consequence of both oxidation (Fig. 11d) and delamination of Pt (Fig. 11c). Lastly, in the case of ML-3 (Fig. 12e), though there is a presence of few nanoscale voids in Ti (highlighted in red circle), the Nb/Ti interface looks sharp, indicating minor penetration of electrolyte to the Ti substrate. Moreover, thickness of Pt and Nb (Fig. 12f) are close to the pristine ML-3, indicating minor damage or oxidation of Nb and Pt. It is to be noted that even though XPS (Fig. S10b) shows the partial oxidation of Ti at Nb/Ti interface in ML-3, it might be related to the thin passivation layer on Ti felt before coating. Nevertheless, multi-layered coatings of ML-2 and ML-3 shows lower corrosion compared to CM-Pt. However, 40.87% of unoxidized Pt (assuming a similar area of retained Pt as ML-2) on CM-Pt explains its higher SLT compared to ML-2, as discussed above.

Among the multi-layered samples i.e. ML-1, ML-2 and ML-3, the order of SLT is consistent with the order of corrosion resistance observed during potentiodynamic and potentiostatic polarization tests. The reason behind the order is explained hereafter. In the case of physical vapor deposition such as sputtering, the density of pinholes and pores is dependent on the thickness of the coating deposited [37]. It has been reported that in the case of sputtered TiN, the density of pinholes decreases from approximately 1000 to 0.1 (number mm^{-2}) on increasing the thickness of TiN from 1.1 µm to 60 µm. Moreover, in another study done by Uchida et al., [38] the area of pinholes decreases from 3.0% to 0.1% when the thickness of TiN is increased from 100 nm to 1000 nm. Therefore, it can be assumed that in the case of ML-1, ML-2 and ML-3, as Nb thickness increases, the density of pinholes in the interlayer

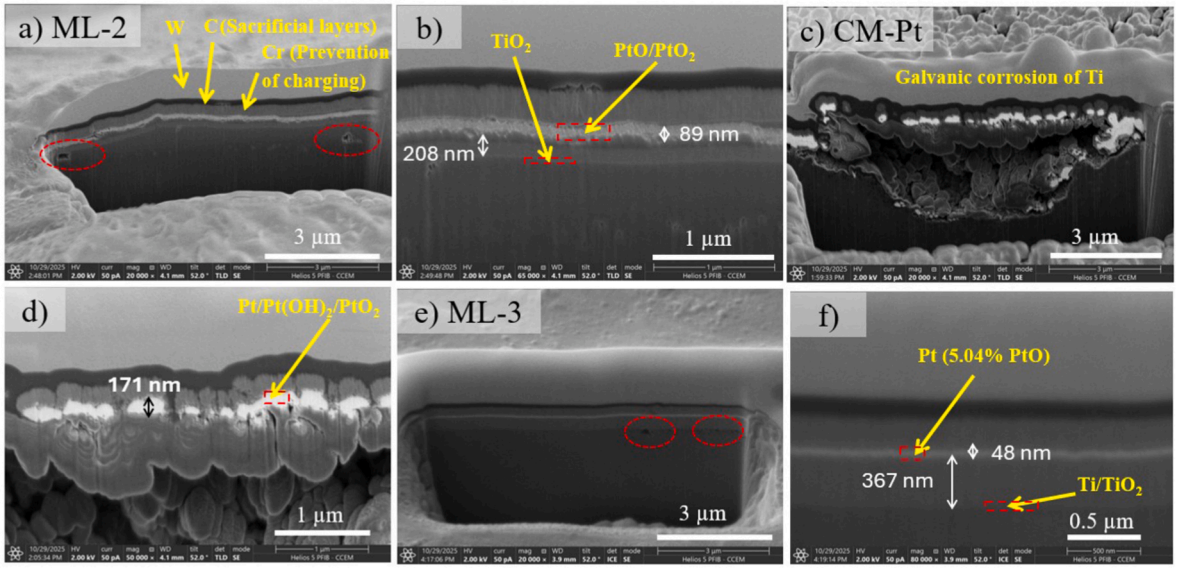

Fig. 12. FIB images of (a, b) ML-2, (c, d) CM-Pt and (e, f) ML-3 after 59 h, 68 h and 68 h, respectively.

decreases, resulting in the higher corrosion resistance. Note that, although the SEM micrograph of ML-2 (Fig. 11a) shows slightly greater peeling than the ML-3 (Fig. 11e), both samples look similar as none of them have shown greater spalling or peeling of the coating. But as seen from cross-section (Fig. 12) and XPS results(Fig. 11), only 5.04% of Pt is oxidized in ML-3 compared to complete oxidation in ML-2, the SLT period turns out to be higher in the case of former than latter. The observed difference in Pt oxidation between ML-2 and ML-3 could be attributed to the disparity in measured voltage corresponding to each sample. As indicated in Fig. 9, both samples start at similar voltage,

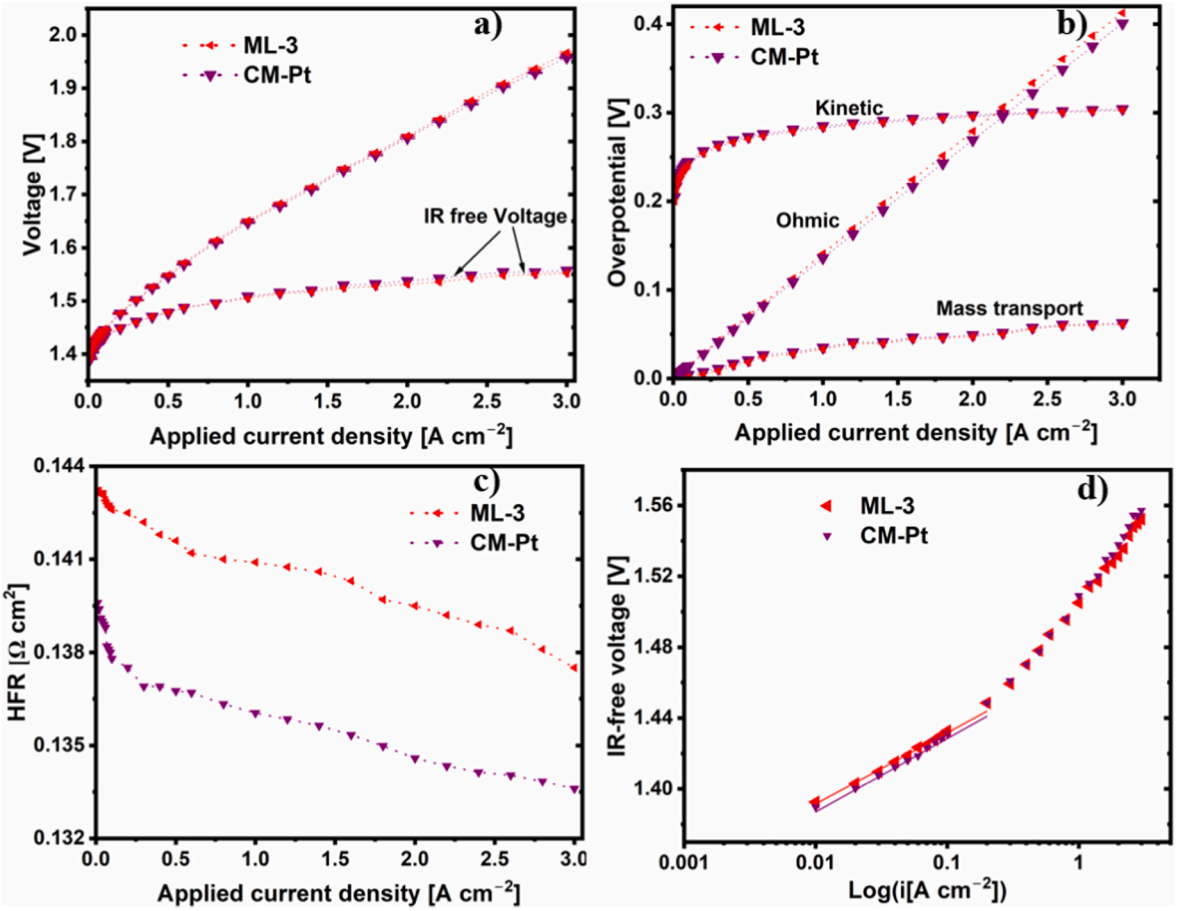

Fig. 13. (a) Polarization curve showcasing the total cell voltage and IR free voltage of ML-3 and CM-Pt (b) Contribution of each of the three overpotentials (ohmic, kinetic and mass transport) for ML-3 and CM-Pt (c) High Frequency Resistance (HFR) for ML-3 and CM-Pt (d) IR-free curve depicting the line fitting to obtain the kinetic overpotential.

however since the early penetration of electrolyte (as confirmed by Fig. S10a) reduces the conductivity in ML-2, higher voltage is required to sustain 2 A cm^{-2}. Hence, compared to ML-3 (~6.5 V), ML-2 remains at higher voltage (~7.5 V) throughout 59 h test, which enhances the rate of Pt oxidation in latter [39,40].

Hence, in consideration of its higher ex-situ performance, ML-3 is compared next with CM-Pt in the in-situ conditions of PEMWE.

3.5. In-situ testing

The single cell performance and the overpotential analyses in the case of ML-3 and CM-Pt are shown in Fig. 13a and b, respectively. It is observed that at 3.0 A cm^{-2}, although ML-3 (1.967 V) shows slightly inferior performance than the CM-Pt (1.958 V), the voltage free from ohmic losses ($V_{IR\text{-}free}$) is lower in the case of former (1.552 V) than the latter (1.557 V). This higher drop in voltage in the case of ML-3 (0.414 V) than that of CM-Pt (0.400 V) is attributed to its higher ohmic overpotential (η_{ohmic}) loss (Fig. 13b), which is subtracted from total cell voltage to obtain $V_{IR\text{-}free}$. Moreover, the higher η_{ohmic} of ML-3 compared to CM-Pt, is in alignment with the trend observed in the ex-situ measurement of ICR (as discussed in section 3.3). But, since the operating conditions such as temperature, current density, materials, pressure etc. is different in both ex-situ as well as in-situ measurement, the values of resistance are different between the two situations [8].

Note that the η_{ohmic}, kinetic (η_{kt}) and mass transport (η_{mt}) overpotential is evaluated by the method adopted by Suermann et al. [41] According to which, η_{ohmic} is calculated by Equation (2),

$$\eta_{ohmic} = I \times HFR \tag{2}$$

where I is the current density and HFR is the corresponding high frequency resistance (Fig. 13c), which is obtained by measuring the x-intercept of high frequency arc in EIS curves (Fig. S11 in the Supplementary Information). As evident from Fig. 13c, the HFR for both ML-3 and CM-Pt samples shows a decreasing trend with increasing current density. This can be explained based on the previous study done by Suermann et al. [41] The authors attributed this decreasing trend of HFR to the enhanced waste heat production at higher current densities. They further reported that irrespective of the pressure difference across the membrane, the trend remained constant, however the rate of decrease in HFR was less pronounced at higher temperature. Nevertheless, according to their findings, the HFR decreased by approximately ~10.0 mΩ cm^2 as current density was increased from 0 to 3.0 A cm^{-2} at 70 °C. Similar range of ΔHFR (~7.0 mΩ cm^2 at 80 °C for ML-3) is observed in our study (Fig. 13c). The slight difference in value could be due to the different operating conditions in both the study. Next, IR-free plot (Fig. 13a) is replotted as Tafel plot, and the tafel equation has been used to fit the curve in low current density region, as shown in Fig. 13d η_{kt} is then derived by deducting thermodynamic cell voltage (Equation (3)) from the fitted line.

$$E^{\circ}\,(\mathrm{V}) = 1.5184\text{–}1.5421 \times 10^{-3}\,T + 9.523 \times 10^{-5}\,T\ln(T) + 9.84 \times 10^{-8}\,T^2 \tag{3}$$

where T (K) is the temperature. Finally, η_{mt} is obtained by deducting the total of η_{kt} and E° from the $V_{IR\text{-}free}$.

As seen from Fig. 13b, despite having similar top layer of Pt in both the cases, ML-3 exhibits lower η_{kt} and η_{mt} compared to CM-Pt. The reason behind this is unclear but could be attributed to the higher toughness and hardness of ML-3 compared to CM-Pt. It has been reported [42] that the deflection of cracks at the interface of multi-layered coatings dissipates energy in the interfacial region, hence enhancing their toughness. In addition to this, the presence of alternate layers of hard (Nb) and soft (Pt) materials would cause the dislocations to pile up at the interfaces [22], resulting in an increase in hardness of the ML-3. Considering this, it can be stated that in the presence of high clamping pressure inside the cell, the tendency of crack initiation and propagation would be higher in the case of CM-Pt compared to ML-3. These cracks in CM-Pt would effectively reduce the contact point of Ti PTL with CL, impacting the catalyst utilization or η_{kt} in the case of membrane swelling. This statement is consistent with the study done by Liu et al., [43] where the authors intentionally left Pt-coatings gaps in thin strips on Ti PTL to study their impact on cell performance. They reported that a reduction in the Pt-coated area led to decreased catalyst utilization, which was reflected by the increase in tafel slopes and η_{kt}. Next, regarding η_{mt}, it has been reported [44] that the cracks generated in Pt-coated PTLs leads to O_2 gas accumulation inside the crack, resulting in delamination of coatings in the simulated PEMWE environment. Similar phenomenon is likely to hold at PTL/CL interface, which could increase the η_{mt} in case of CM-Pt due to its higher tendency of crack formation than multi-layered ML-3, as discussed above.

It is worth mentioning that although the total thickness of ML-3 (Nb = 350 nm, Pt = 50 nm) is higher than CM-Pt (Pt = 200 nm), the cost of the coatings is lower in the case of former than the latter. This is attributed to the significant price difference between the Pt and Nb, i.e. as per March 2025, the cost of Pt and Nb is 32247.20 USD kg^{-1}, and 81.10 USD kg^{-1}, respectively. Note that since coating represents a major proportion of overall manufacturing cost of PTL, the impact of these price differences becomes particularly important on a large industrial scale. According to National renewable energy laboratory (USA) [45], the cost contribution of PVD's coating has increased from ~50% to ~60% from 2019 to 2024 at a production rate exceeding 1000 units/year. However, since both samples (CM-Pt and ML-3) are produced through different methodology i.e. electroplating (non-PVD) and sputtering (PVD), respectively, it's important to understand the total cost of both coating methods to ensure a fair comparison to CAPEX. Merlo et al. [46] reported that for depositing 20 μm-thick Cr coating on 1.0 m^2 cylindrical area, although the electricity and equipment costs were greater for magnetron sputtering, its labor cost was comparatively lower than that of electroplating. This resulted in similar cost outcome. Assuming the same to be true for industrial PTL (0.1–0.3 m^2) the difference in CAPEX would solely be due to the price variation in the coating material. Hence, considering the coating price, mentioned above, 200 nm of Pt replaced with 50 nm of Pt and 350 nm of Nb would amount to ~75% decrease in cost of coating and ~45% reduction in overall manufacturing cost of PTL. It is to be noted that while Nb has shown considerable potential in the present study, it has been regarded as critical raw material by European commission in 2023 [47]. In addition, ~99% of Nb production are concentrated in Brazil and Canada, highlighting its geographical scarcity. Hence, to limit the Nb usage, the more abundant alternatives such as Zr, V etc. (having high oxygen affinity) need to be investigated in combination with Nb. For instance, addition of 1%Nb in Zr has shown to improve its corrosion resistance and is being widely used in nuclear reactors [48].

4. Conclusions

In this study, Nb was investigated as an interlayer between thin layer of Pt coating (50 nm) and Ti PTL to reduce the overall cost of commercial Pt coated (200 nm) Ti PTL. Three different thicknesses of Nb interlayer were deposited and was compared with two single layered Pt samples i.e. SL-Pt (having similar Pt loading) and commercial CM-Pt (having higher Pt loading) in both ex-situ as well as in-situ conditions of PEMWE. The results showed that the samples with Nb as an interlayer (ML-1, ML-2 and ML-3) performed better than the sample without interlayer (SL-Pt) in a PEMWE simulated conditions. This was attributed to the inhibition of galvanic corrosion and the better adhesion of Pt with Nb than that with Ti in the case of multi-layered samples compared to single layered, SL-Pt. Next, it was observed that with the increase in the thickness of Nb interlayer, the SLT of the multi-layered samples increased in the following order i.e. ML-1 (45 h) < ML-2 (59 h) < ML-3 (102 h). This was due to the higher amount of peeling in ML-1 compared to ML-2 and the complete oxidation of Pt in ML-2 compared to ML-3 (5.04 %).

Nevertheless, the ICR of all the multi-layered samples after CA were found to be quite low (<10 mΩ cm^2) in the entire range of 1.2–2.0 MPa.

Compared to commercial CM-Pt sample, only ML-3 demonstrated higher SLT than the former, which could be attributed to the higher number of pinholes in ML-1 and ML-2 compared to ML-3. The in-situ results indicated that multi-layered ML-3 showed slightly lower performance (1.967 V@3.0 A cm^{-2}) than CM-Pt (1.958 V@3.0 A cm^{-2}). This was due to the higher ohmic overpotential in the case of ML-3 than CM-Pt, which opens door for the future work to lower the HFR in the case of former. The results obtained from this study effectively emphasize the importance of a Nb based middle layer for increased durability and an economically feasible pathway for PTL coating fabrication with low Pt utilization.

CRediT authorship contribution statement

Anurag: Writing – original draft, Visualization, Validation, Methodology, Investigation, Formal analysis, Conceptualization. **Abhay Gupta:** Writing – review & editing, Visualization, Validation, Methodology. **Samaneh Shahgaldi:** Writing – review & editing, Supervision, Resources, Project administration, Methodology, Funding acquisition, Conceptualization.

Declaration of competing interest

The authors declare that they have no known competing financial interests or personal relationships that could have appeared to influence the work reported in this paper.

Acknowledgements

Shahgaldi research team at the Hydrogen Research Institute, University of Quebec a Trois Rivières would like to acknowledge the support of the Natural Sciences and Engineering Research Council of Canada (NSERC), Canada Research Chair (CRC-2019-00354), Discovery grant (CRSNG-DGECR-2022-00058), Prima Quebec (R23-13-005), NSERC-Alliance (3289542) and Mitacs Accelerate (IT30506). The authors would like to thank Niobay team for their constant support.

Appendix A. Supplementary data

Supplementary data to this article can be found online at https://doi.org/10.1016/j.renene.2026.125373.

Nomenclature

E_{corr}	corrosion potential, V
I_{corr}	corrosion current density, μA cm^{-2}
β_a, β_c	tafel slopes, mV $decade^{-1}$
R_P	polarization resistance, Ω cm^{-2}
$V_{IR\text{-}free}$	IR-free voltage, V
HFR	high frequency resistance, Ω cm^{-2}
I	current density, A cm^{-2}
η_{ohmic}	ohmic overpotential, V
η_{kt}	kinetic overpotential, V
η_{mt}	mass transport overpotential, V
E°	thermodynamic cell voltage, V

Abbreviations

PTLs	porous transport layers
PEMWEs	proton exchange membrane water electrolyzers
MEA	membrane electrode assembly
OPEX	operation expenditure
CAPEX	capital expenditure
PGMs	pt-group metals
BPPs	bipolar plates
ICR	interfacial contact resistance
OCP	open circuit potential
CA	chronoamperometry
SLT	simulated lifetime
SEM	scanning electron microscopy
EDS	energy dispersive x-ray spectroscopy
XPS	x-ray photoelectron spectroscopy
GDLs	gas diffusion layers
EIS	electrochemical impedance spectroscopy
BSE	backscattered electron
OER	oxygen evolution reaction

Data availability

Data will be made available on request.

References

[1] G.W. Crabtree, M.S. Dresselhaus, M.V. Buchanan, The hydrogen economy, Phys. Today 57 (2004) 39–44, https://doi.org/10.1063/1.1878333.
[2] L. Moradizadeh, P.V. Madhavan, Y.M. Chellehbari, A. Gupta, X. Li, S. Shahgaldi, Porous transport layers with low Pt loading having Nb–Ta alloy as interlayer for proton exchange membrane water electrolyzers, Int. J. Hydrogen Energy 94 (2024) 1114–1129, https://doi.org/10.1016/J.IJHYDENE.2024.11.192.
[3] Y. Tang, S. Su, X. Niu, Z. Song, W. Li, A gradient porous transport layer enabling a high-performance proton-exchange membrane electrolysis cell, Renew. Energy 237 (2024) 121707, https://doi.org/10.1016/J.RENENE.2024.121707.
[4] C. Kim, S. Seo, S. Yoon, J. Kim, Y. Park, P. Lee, D. You, Effects of oxygen bubble formation in the porous transport layer on the performance of polymer-electrolyte-membrane water electrolyzer, Renew. Energy 256 (2026) 124194, https://doi.org/10.1016/J.RENENE.2025.124194.
[5] Z. Wang, X. Wang, H. Guo, T. Wang, X. Li, S. Liu, C. Xu, K. Wang, A two-dimensional numerical study of oxygen transport in porous transport layer of PEMEC using the phase field method, Renew. Energy 247 (2025) 123044, https://doi.org/10.1016/J.RENENE.2025.123044.
[6] K. Chen, Z. Xiong, D. He, Z. Luo, G. Zou, W. Chen, B. Chen, Optimization of porous transport layer for overall performance improvement in unitized regenerative fuel cell under clamping pressures, Renew. Energy 251 (2025) 123459, https://doi.org/10.1016/J.RENENE.2025.123459.
[7] Z. Kang, G. Yang, J. Mo, Development of an ultra-thin electrode for the oxygen evolution reaction in proton exchange membrane water electrolyzers, Renew. Energy 224 (2024) 120159, https://doi.org/10.1016/J.RENENE.2024.120159.
[8] C. Rakousky, U. Reimer, K. Wippermann, M. Carmo, W. Lueke, D. Stolten, An analysis of degradation phenomena in polymer electrolyte membrane water electrolysis, J. Power Sources 326 (2016) 120–128, https://doi.org/10.1016/j.jpowsour.2016.06.082.
[9] C. Rakousky, G.P. Keeley, K. Wippermann, M. Carmo, D. Stolten, The stability challenge on the pathway to high-current-density polymer electrolyte membrane water electrolyzers, Electrochim. Acta 278 (2018) 324–331, https://doi.org/10.1016/J.ELECTACTA.2018.04.154.
[10] C. Liu, M. Carmo, G. Bender, A. Everwand, T. Lickert, J.L. Young, T. Smolinka, D. Stolten, W. Lehnert, Performance enhancement of PEM electrolyzers through iridium-coated titanium porous transport layers, Electrochem. Commun. 97 (2018) 96–99, https://doi.org/10.1016/j.elecom.2018.10.021.
[11] S. Stiber, H. Balzer, A. Wierhake, F.J. Wirkert, J. Roth, U. Rost, M. Brodmann, J. K. Lee, A. Bazylak, W. Waiblinger, A.S. Gago, K.A. Friedrich, Porous transport layers for proton exchange membrane electrolysis under extreme conditions of current density, temperature, and pressure, Adv. Energy Mater. 11 (2021), https://doi.org/10.1002/aenm.202100630.
[12] P. Lettenmeier, S. Kolb, F. Burggraf, A.S. Gago, K.A. Friedrich, Towards developing a backing layer for proton exchange membrane electrolyzers, J. Power Sources 311 (2016) 153–158, https://doi.org/10.1016/J.JPOWSOUR.2016.01.100.
[13] H. Ye, Z. Tu, S. Li, Electrochemical performance of metal nitride coated titanium bipolar plate for proton exchange membrane water electrolyser, J. Power Sources 595 (2024), https://doi.org/10.1016/j.jpowsour.2024.234052.
[14] H. Ye, L. Chen, D. Shen, S. Li, Z. Tu, Performance of Ta/TaN coated titanium felt for proton exchange membrane water electrolysis, Int. J. Hydrogen Energy 93 (2024) 1022–1030, https://doi.org/10.1016/J.IJHYDENE.2024.11.057.
[15] T. Deng, H. Huang, L. Fan, S. Xu, H. Li, Porous transport layers with TiC-Coated microporous layers for proton exchange membrane water electrolysis, ACS Sustain. Chem. Eng. 11 (2023) 17075–17085, https://doi.org/10.1021/ACSSUSCHEMENG.3C05256/ASSET/IMAGES/MEDIUM/SC3C05256_0013.GIF.
[16] Z. Fan, H. Yu, G. Jiang, D. Yao, S. Sun, J. Chi, B. Qin, Z. Shao, Low precious metal loading porous transport layer coating and anode catalyst layer for proton exchange membrane water electrolysis, Int. J. Hydrogen Energy 47 (2022) 18963–18971, https://doi.org/10.1016/J.IJHYDENE.2022.04.114.
[17] T.L. Doan, H.E. Lee, M.J. Kim, W.C. Cho, H.S. Cho, T. Kim, Influence of IrO2/TiO2 coated titanium porous transport layer on the performance of PEM water

electrolysis, J. Power Sources 533 (2022) 231370, https://doi.org/10.1016/J.JPOWSOUR.2022.231370.
[18] Y. Liu, S. Huang, D. Wang, H. Zhang, D. Shan, S. Peng, G. Shen, L. Wang, X. Wang, Modifying Ti-Based gas diffusion layer passivation for polymer electrolyte membrane water electrolysis via electrochemical nitridation, ACS Appl. Mater. Interfaces 14 (2022) 15728–15735, https://doi.org/10.1021/ACSAMI.1C22639.
[19] C.M. Hwang, M. Ishida, H. Ito, T. Maeda, A. Nakano, A. Kato, T. Yoshida, Effect of titanium powder loading in gas diffusion layer of a polymer electrolyte unitized reversible fuel cell, J. Power Sources 202 (2012) 108–113, https://doi.org/10.1016/J.JPOWSOUR.2011.11.041.
[20] N.F. Daudt, A.D. Schneider, E.R. Arnemann, C.J. Scheuer, L.S. Dorneles, L. F. Schelp, N.F. Daudt, A.D. Schneider, E.R. Arnemann, C.J. Scheuer, L.S. Dorneles, L.F. Schelp, Fabrication of NbN-Coated porous titanium sheets for PEM electrolyzers, JMEP 29 (2020) 5174–5183, https://doi.org/10.1007/S11665-020-05026-Y.
[21] C.A. Huang, S.W. Yang, P.L. Lai, Effect of precursor baking on the electrochemical properties of IrO2-Ta2O5/Ti anodes, Surf. Coat. Technol. 350 (2018) 896–903, https://doi.org/10.1016/J.SURFCOAT.2018.03.095.
[22] S.J. Bull, A.M. Jones, Multilayer coatings for improved performance, Surf. Coat. Technol. 78 (1996) 173–184, https://doi.org/10.1016/0257-8972(94)02407-3.
[23] H. Holleck, M. Lahres, P. Woll, Multilayer coatings—influence of fabrication parameters on constitution and properties, Surf. Coat. Technol. 41 (1990) 179–190, https://doi.org/10.1016/0257-8972(90)90166-A.
[24] D. Zhou, H. Peng, L. Zhu, H. Guo, S. Gong, Microstructure, hardness and corrosion behaviour of Ti/TiN multilayer coatings produced by plasma activated EB-PVD, Surf. Coat. Technol. 258 (2014) 102–107, https://doi.org/10.1016/J.SURFCOAT.2014.09.058.
[25] Y.L. Chipatecua, J.J. Olaya, D.F. Arias, Corrosion behaviour of CrN/Cr multilayers on stainless steel deposited by unbalanced magnetron sputtering, Vacuum 86 (2012) 1393–1401, https://doi.org/10.1016/J.VACUUM.2012.01.016.
[26] A. Singh, B.S. De, S. Singh, S.P. Thota, M. Khalid, S. Shahgaldi, Exploring the engineered electroplating process for coating of gold on the inner structure of porous transport layer (PTL): performance evaluation of coating in simulated PEM electrolyzer, Int. J. Hydrogen Energy 106 (2025) 1029–1040, https://doi.org/10.1016/J.IJHYDENE.2025.02.047.
[27] A. Endrikat, N. Borisenko, A. Ispas, R. Peipmann, F. Endres, A. Bund, Electrochemical reduction mechanism of NbF5 and NbCl5 in the ionic liquid 1-butyl-1-methylpyrrolidinium trifluoromethanesulfonate, Electrochim. Acta 321 (2019) 134600, https://doi.org/10.1016/J.ELECTACTA.2019.134600.
[28] US4632734A - Process for electrochemically or chemically coating niobium - google patents, (n.d.). https://patents.google.com/patent/US4632734A/en (accessed November 9, 2025).
[29] Literature review of Nb Electroplating – Dmytro chirkov – TFSRF-2010 – surface technologies and superconductivity service, (n.d.). https://surfacetreatments.infn.it/literature-review-of-nb-electroplating-dmytro-chirkov-tfsrf-2010/(accessed November 9, 2025).
[30] A. Gupta, Y.M. Chellehbari, S. Shahgaldi, Achieving high performance and durability with ultra-low precious metal nanolayer on porous transport layer for PEMWE application, J. Power Sources 630 (2025) 236088, https://doi.org/10.1016/J.JPOWSOUR.2024.236088.
[31] C. Liu, K. Wippermann, M. Rasinski, Y. Suo, M. Shviro, M. Carmo, W. Lehnert, Constructing a multifunctional interface between membrane and porous transport layer for water electrolyzers, ACS Appl. Mater. Interfaces 13 (2021) 16182–16196, https://doi.org/10.1021/acsami.0c20690.
[32] J. Marien, T. Wagner, G. Duscher, A. Koch, M. Rühle, Nb on (110) TiO2 (rutile): growth, structure, and chemical composition of the interface, Surf. Sci. 446 (2000) 219–228, https://doi.org/10.1016/S0039-6028(99)01172-3.
[33] A. Erdemir, R.A. Erck, Effect of niobium interlayer on high-temperature sliding friction and wear of silver films on alumina, Tribol. Lett. 2 (1996) 23–36, https://doi.org/10.1007/BF00182545/METRICS.
[34] Y. Mehdizadeh Chellehbari, L. Moradizadeh, M. Johar, A. Gupta, X. Li, S. Shahgaldi, Evaluation of niobium-based bipolar plates with ultra-low precious metal coatings for high-performance and durable PEM water electrolyzers, Mater. Today Energy 51 (2025) 101913, https://doi.org/10.1016/J.MTENER.2025.101913.
[35] Y. Abe, M. Kawamura, K. Sasaki, Preparation of PtO and α-PtO2 thin films by reactive sputtering and their electrical properties, Jpn. J. Appl. Phys. 38 (1999) 2092–2096, https://doi.org/10.1143/JJAP.38.2092.
[36] Z. Feng, G.L. Song, Y. Xu, D. Zheng, X. Chen, Micro-galvanic corrosion during formation of epoxy coating, Prog. Org. Coating 147 (2020) 105799, https://doi.org/10.1016/J.PORGCOAT.2020.105799.
[37] H.A. Jehn, Improvement of the corrosion resistance of PVD hard coating–substrate systems, Surf. Coat. Technol. 125 (2000) 212–217, https://doi.org/10.1016/S0257-8972(99)00551-4.
[38] H. Uchida, S. Inoue, K. Koterazawa, Electrochemical evaluation of pinhole defects in TiN films prepared by r.f. reactive sputtering, Mater. Sci. Eng., A 234–236 (1997) 649–652, https://doi.org/10.1016/S0921-5093(97)00233-5.
[39] M. Grdeń, Platinum oxidation in alkaline electrolyte under potentiostatic conditions, Electrochem. Commun. 61 (2015) 14–17, https://doi.org/10.1016/J.ELECOM.2015.09.017.
[40] R. Mom, L. Frevel, J.J. Velasco-Vélez, M. Plodinec, A. Knop-Gericke, R. Schlögl, The oxidation of platinum under wet conditions observed by electrochemical X-ray Photoelectron spectroscopy, J. Am. Chem. Soc. 141 (2019) 6537–6544, https://doi.org/10.1021/JACS.8B12284.
[41] M. Suermann, T.J. Schmidt, F.N. Büchi, Cell performance determining parameters in high pressure water electrolysis, Electrochim. Acta 211 (2016) 989–997, https://doi.org/10.1016/J.ELECTACTA.2016.06.120.
[42] K.S. Chan, M.Y. He, J.W. Hutchinson, Cracking and stress redistribution in ceramic layered composites, Mater. Sci. Eng. 167 (1993) 57–64, https://doi.org/10.1016/0921-5093(93)90337-E.
[43] C. Liu, J.A. Wrubel, E. Padgett, G. Bender, Impacts of PTL coating gaps on cell performance for PEM water electrolyzer, Appl. Energy 356 (2024) 122274, https://doi.org/10.1016/J.APENERGY.2023.122274.
[44] L. Jing, J. Wu, L. Li, L. Chang, X. Lu, X. Li, X. Sun, L. Ma, J. Hao, G. Zhang, Z. Deng, J. Yao, D. Jing, Unveiling the failure mechanism of Pt coating on Ti porous transport layer in simulated PEMEC environment, ACS Appl. Mater. Interfaces 17 (2025) 51105–51117, https://doi.org/10.1021/ACSAMI.5C08467.
[45] A. Badgett, J. Brauch, A. Thatte, R. Rubin, C. Skangos, X. Wang, R. Ahluwalia, B. Pivovar, M. Ruth, Updated manufactured cost analysis for Proton exchange membrane water electrolyzers. www.nrel.gov/publications, 2023.
[46] A. Merlo, G. Léonard, Magnetron sputtering vs. Electrodeposition for hard chrome coatings: a comparison of environmental and economic performances, Materials 14 (2021), https://doi.org/10.3390/MA14143823/S1.
[47] Milan Grohol, Constanze Veeh, Study on the Critical Raw Materials for the EU 2023, final report, 2023, p. 152.
[48] A.V. Nikulina, Zirconium-niobium alloys for core elements of pressurized water reactors, Met. Sci. Heat Treat. 45 (2003) 287–292, https://doi.org/10.1023/A:1027388503837/METRICS.